J|A|C|S
ARTICLES

Published on Web 05/28/2009

Helical Vesicles, Segmented Semivesicles, and Noncircular Bilayer Sheets from Solution-State Self-Assembly of ABC Miktoarm Star Terpolymers

Weixin Kong,[†] Baohui Li,*[,†] Qinghua Jin,[†] Datong Ding,[†] and An-Chang Shi*[,‡]

College of Physics and Key Laboratory of Functional Polymer Materials of Ministry of Education, Nankai University, Tianjin, 300071, China, and Department of Physics and Astronomy, McMaster University, Hamilton, Ontario L8S 4M1, Canada

Received January 19, 2009; E-mail: baohui@nankai.edu.cn; shi@mcmaster.ca

Abstract: Multicompartment micelles, especially nanostructured vesicles, offer tremendous potential as delivery vehicles of therapeutic agents and nanoreactors. Solution-state self-assembly of miktoarm star terpolymers provides a versatile and powerful route to obtain multicompartment micelles. Here we report simulations of solution-state self-assembly of ABC star terpolymers composed of a solvophilic A arm and two solvophobic B and C arms. A variety of multicompartment micelles are predicted from the simulations. Phase diagrams for typical star terpolymers are constructed. It is discovered that the overall micelle morphology is largely controlled by the volume fraction of the solvophilic A arms, whereas the internal compartmented and/or segregated structures depend on the ratio between the volume fractions of the two solvophobic arms. The polymer−solvent and polymer−polymer interactions can be used to tune the effective volume fraction of the A-arm and, thereby, induce morphological transitions. For terpolymers with equal or nearly equal length of B and C arms, several previously unknown structures, including vesicles with novel lateral structures (helices or stacked donuts), segmented semivesicles, and elliptic or triangular bilayer sheets, are discovered. When the lengths of B and C arms are not equal, novel micelles such as multicompartment disks and onions are observed.

Introduction

One of the bottom-up strategies of creating structured materials for nanotechnology is to utilize spontaneous self-assembly of macromolecules. It has been proposed that the self-assembly of amphiphilic molecules into supramolecular assemblies and ordered structures can be used in the development of many new nanotechnological applications such as nanolithography,[1] biomineralization,[2] and drug delivery.[3] The key to the success of this bottom-up strategy is the ability to predict and control the self-assembled nanostructures from the building molecules. One promising class of building molecules for nanoscale templates is block copolymers, which are macromolecules formed by covalently linking two or more chemically distinct polymeric blocks. In recent years, it has been demonstrated that block copolymers can be used to engineer a host of novel structures by tuning the block lengths, polymer architecture, and the type of monomers. The formation of ordered periodic structures and various micellar morphologies from block copolymer melts and solutions is well documented.[4,5]

While the formation of ordered periodic phases from block copolymer melts is largely controlled by the polymer architecture, block length, and monomer−monomer interactions, the existence of selective solvents leads to extra controlling parameters such as solvent−polymer interactions and polymer concentration. The self-assembly of block copolymers in selective solvents is of fundamental interest because it offers tremendous promise for the creation of nanostructured materials in the form of micelles of different shape and internal structure.[5] These nanostructured materials can potentially be used in advanced applications in diverse areas such as nanoreactors, biological function, and drug delivery. Furthermore, these structures have strong biological implications in that they are analogies of assemblies formed from biopolymers and lipids.

The simplest block copolymers are AB diblock copolymers, composed of two blocks (A and B) linked at their ends. In the past years, the self-assembly of AB diblock (and ABA triblock) copolymers in solutions has been extensively investigated,[5−9] revealing a wide range of different micellar morphologies (spheres, rods, vesicles, and reverse micellar assemblies). On the other hand, the morphologies formed with block copolymers composed of two types of monomers, such as AB diblock or ABA triblock copolymers, are limited to those structures formed

[†] Nankai University.
[‡] McMaster University.

(1) Park, M.; Harrison, C.; Chaikin, P. M.; Register, R. A.; Adamson, D. H. *Science* **1997**, *276*, 1401.
(2) Collier, J. H.; Messersmith, P. B. *Annu. Rev. Mater. Res.* **2001**, *31*, 237.
(3) Savic, M. R.; Luo, L.; Eisenberg, A.; Maysinger, D. *Science* **2003**, *300*, 615.
(4) Hamley, I. W. *The Physics of Block Copolymers*; Oxford University Press: New York, 1998.
(5) Hamley, I. W. *Block Copolymers in Solution: Fundamentals and Applications*; Wiley: Hoboken, NJ, 2005.
(6) Gohy, J. F. *Adv. Polym. Sci.* **2005**, *190*, 65.
(7) Riess, G. *Prog. Polym. Sci.* **2003**, *28*, 1107.
(8) Zhang, L.; Eisenberg, A. *Science* **1995**, *268*, 1728.
(9) Jain, S.; Bates, F. S. *Science* **2003**, *300*, 460.

by partitioning the space into two ("inside" and "outside") domains. A possibility to break this two-domain barrier is to utilize block copolymers composed of three or more types of monomers. It has been demonstrated that partitioning the space into three or more domains provides the possibility of forming multicompartment micellar structures.[10−26] Generically, the micellar structures formed from multiblock copolymers in selective solvents are composed of solvophilic and solvophobic domains. The solvophobic domain can be further divided into distinct nanoscopic subdomains, leading to the formation of multicompartment micelles. The possibility of forming multicompartment micelles from block copolymers represents a significant step toward achieving hierarchical self-assembly with multiple functions and designed architectural features at several length scales.[17]

Multicompartment micelles can be formed from linear multiblock copolymers with two or more solvophobic blocks, such as linear ABC triblock,[12] ABCA tetrablock,[13] and ABCBA pentablock[14] copolymers. A generic feature of the structures from linear block copolymers is that the junctions connecting two different blocks are forced to be on the interfaces between the two different domains. As a result of this topological constraint, a concentric arrangement of core−shell−corona domains is usually obtained for linear ABC triblock copolymers, regardless of the overall micellar shape.[16,23] On the other hand, the polymeric architecture of miktoarm star copolymers, in which three or more different blocks are linked at one junction point, requires that these junction points lie on the mutual intersections of different domains. For example, the junction points in the structures formed by ABC star terpolymers will lie on the mutual intersections of the A, B, and C domains. This topological requirement can effectively suppress the formation of concentric domains, leading to the formation of more complex multicompartment micelles. The ability of ABC star terpolymers to form rich and complex micellar structures has been clearly demonstrated in recent experimental studies by Lodge and co-workers.[16−19] Specifically, Lodge et al. have observed a variety of fascinating multicompartment micelles, including laterally nanostructured vesicles and bowl shaped semivesicles, polygonal shaped bilayer sheets, segmented wormlike micelles, hamburger micelles, and raspberry micelles, from the self-assembly of [poly(ethylethylene)]-[poly(ethylene oxide)]-[poly(perfluoropropylene oxide)] (termed μ-EOF) miktoarm star terpolymers in aqueous solutions.[16−18] They also noticed that the nanostructured vesicles, semivesicles, and bilayer sheets are usually with protruding tails.[17] Furthermore, experimental morphology diagrams, revealing morphological transition sequences, have been obtained by systematically changing the block lengths. Besides these extensive experimental investigations, simulation and theoretical studies of solution-state self-assembly of ABC star terpolymers have also been performed by a few groups.[20−24] Zhong et al.[20] and Chou et al.[21] carried out dissipative particle dynamics simulations and observed hamburger micelles, segmented worms, and Y-junctions. Zhu et al.[22] performed Monte Carlo simulations and obtained wormlike pearl-necklace micelles and compact or incompact micelles. On the theoretical side, Ma et al.[23] carried out a two-dimensional real-space self-consistent field theory calculation and obtained various micellar structures including bead-on-string worm, raspberry, hamburger, segmented worm-like, toroidal segmented micelles, and vesicles. Very recently, Zhulina and Borisov[24] published a scaling analysis of micelles from ABC star terpolymers and predicted stable starlike micelles and cylindrical crew-cut micelles. Multicompartment micelles have also been observed or predicted to spontaneously form in blends of ABC star terpolymers and AB or ABC linear block copolymers[23,25,26] or in blends of two different diblock copolymers.[27]

Despite these previous studies, a comprehensive understanding of the spontaneous self-assembly of complex morphologies from ABC star terpolymers in selective solvents still presents a challenging task to the physical chemistry community. Specifically, exploring the huge phase space, which is defined by the large number of parameters controlling the morphology of ABC star terpolymer solutions, requires the ability to systematically vary the terpolymer compositions and monomer−monomer interactions. Extensive experimental efforts, exemplified by the work of Lodge and co-workers, provide valuable contributions to the understanding of the complex morphologies of self-assembled ABC star terpolymers. On the other hand, because varying copolymer compositions and monomer−monomer interactions involve the synthesis of a large number of block copolymers, experimental exploration of the phase space is a very costly and time-consuming task. In addition, identifying fine structures and chain conformation presents another experimental challenge. From this perspective, theory and simulation provide an ideal tool for the investigation of the phase behavior of ABC terpolymers and for the elucidation of fine structures and chain packing. In particular, theory and simulations can be used to obtain a good understanding of the detailed relationship between the micellar structure and molecular parameters (block type, composition, architecture, and interactions). This relation-

(10) Laschewsky, A. *Curr. Opin. Colloid Interface Sci.* **2003**, *8*, 274.
(11) Lutz, J.-F.; Laschewsky, A. *Macromol. Chem. Phys.* **2005**, *206*, 813.
(12) (a) Yu, G.; Eisenberg, A. *Macromolecules* **1998**, *31*, 5546. (b) Gohy, J.-F.; Willet, N.; Varshney, S.; Zhang, J.-X.; Jérôme, R. *Angew. Chem., Int. Ed.* **2001**, *40*, 3214. (c) Zhou, Z.; Li, Z.; Ren, Y.; Hillmyer, M. A.; Lodge, T. P. *J. Am. Chem. Soc.* **2003**, *125*, 10182. (d) Lodge, T. P.; Hillmyer, M. A.; Zhou, Z.; Talmon, Y. *Macromolecules* **2004**, *37*, 6680. (e) Pochan, D. J.; Chen, Z.; Cui, H.; Hales, K.; Qi, K.; Wooley, K. L. *Science* **2004**, *306*, 94. (f) Kubowicz, S.; Baussard, J.-F.; Lutz, J.-F.; Thünemann, A. F.; von Berlepsch, H.; Laschewsky, A. *Angew. Chem., Int. Ed.* **2005**, *44*, 5262. (g) Zhu, J.; Jiang, W. *Macromolecules* **2005**, *38*, 9315. (h) Li, Z.; Chen, Z.; Cui, H.; Hales, K.; Qi, K.; Wooley, K. L.; Pochan, D. J. *Langmuir* **2005**, *21*, 7533. (i) Chen, Z.; Cui, H.; Hales, K.; Li, Z.; Qi, K.; Pochan, D. J.; Wooley, K. L. *J. Am. Chem. Soc.* **2005**, *127*, 8592. (j) Fustin, C.-A.; Abetz, V.; Gohy, J.-F. *Eur. Phys. J. E* **2005**, *16*, 291.
(13) (a) Brannan, A. K.; Bates, F. S. *Macromolecules* **2004**, *37*, 8816. (b) Gomez, E. D.; Rappl, T. J.; Agarwal, V.; Bose, A.; Schmutz, M.; Marques, C. M.; Balsara, N. P. *Macromolecules* **2005**, *38*, 3567.
(14) Thünemann, A. F.; Kubowicz, S.; von Berlepsch, H.; Möhwald, H. *Langmuir* **2006**, *22*, 2506.
(15) Kubowicz, S.; Thünemann, A. F.; Weberskirch, R.; Möhwald, H. *Langmuir,* **2005**, *21*, 7214.
(16) Li, Z.; Kesselman, E.; Talmon, Y.; Hillmyer, M. A.; Lodge, T. P. *Science* **2004**, *306*, 98.
(17) Li, Z.; Hillmyer, M. A.; Lodge, T. P. *Nano Lett.* **2006**, *6*, 1245.
(18) Li, Z.; Hillmyer, M. A.; Lodge, T. P. *Langmuir* **2006**, *22*, 9409.
(19) (a) Saito, N.; Liu, C.; Lodge, T. P.; Hillmyer, M. A. *Macromolecules* **2008**, *41*, 8815. (b) Liu, C.; Hillmyer, M. A.; Lodge, T. P. *Langmuir* **2008**, *24*, 12001.
(20) (a) Xia, J.; Zhong, C. *Macromol. Rapid Commun.* **2006**, *27*, 1110. (b) Zhong, C.; Liu, D. *Macromol. Theory Simul.* **2007**, *16*, 141.
(21) Chou, S.-H.; Tsao, H.-K.; Sheng, Y.-J. *J. Chem. Phys.* **2006**, *125*, 194903.
(22) Zhu, Y.; Li, R. K. Y.; Jiang, W. *Chem. Phys.* **2006**, *327*, 137.
(23) Ma, J. W.; Li, X.; Tang, P.; Yang, Y. L. *J. Phys. Chem. B* **2007**, *111*, 1552.
(24) Zhulina, E. B.; Borisov, O. V. *Macromolecules* **2008**, *41*, 5934.
(25) Li, Z.; Hillmyer, M. A.; Lodge, T. P. *Macromolecules* **2006**, *39*, 765.
(26) Xin, J.; Liu, D.; Zhong, C. *J. Phys. Chem. B* **2007**, *111*, 13675.
(27) (a) Srinivas, G.; Pitera, J. W. *Nano Lett.* **2008**, *8*, 611. (b) Zhu, J.; Hayward, R. C. *Macromolecules* **2008**, *41*, 7794.

ship is central to the engineering of new micelle structures with potentially enhanced properties and functionalities.

In this paper, we report an extensive investigation of the solution-state self-assembly of amphiphilic ABC star terpolymers using computer simulations. The advantage of computer simulations is that varying the polymer composition and interactions can be easily achieved, allowing the exploration of the phase space to an unprecedented extent. In the simulations, a rich variety of multicompartment micelles are formed spontaneously from a randomly generated initial state. In particular, a host of bilayer membrane-based structures (vesicles, semivesicles, or sheets) with complex microphase separated morphologies are predicted. The effects of terpolymer composition, solvent quality, and incompatibility between the two solvophobic arms on the morphologies and morphological transitions are examined systematically. These simulations complement the existing experimental and theoretical results, leading to a more complete understanding of the phase behavior of ABC star terpolymers in selective solvents.

Model and Method

The computer simulations were performed using a simulated annealing method, which is a well-known procedure for obtaining the lowest-energy "ground states" in complex systems.[28] In the model system the polymers are presented by the single-site bond fluctuation model.[29,30] The combination of the lattice model and simulated annealing method is known to provide an efficient methodology for studying the self-assembly of block copolymers in solutions[31] or in confined environments.[32] For completeness, the model and algorithm are briefly reviewed below, whereas a detailed description can be found elsewhere.[31]

The polymers and solvents are embedded in a simple cubic lattice of volume $V = L \times L \times L$ ($L = 60$) with periodic boundary conditions applied to all three directions. Each star terpolymer molecule consists of three (A, B, and C) arms and a junction point. The i-th arm is a chain with N_i monomers of type i (i = A, B, and C). The junction point is a monomer of type D, which is bonded to the ends of the A, B, and C arms. Thus the total number of monomers of each terpolymer molecule is $N = N_A + N_B + N_C + 1$. Each monomer occupies one lattice site, and two consecutive monomers are connected by bonds that can adopt a length of 1 or $\sqrt{2}$. Therefore each lattice site has 18 nearest neighbor sites. The terpolymers are assumed to be self-avoiding; thus no two monomers can occupy the same site simultaneously. The initial configuration is generated by randomly creating a desired number of terpolymer molecules on the lattice. After the desired number of terpolymer molecules has been generated, the unoccupied sites are designated as solvent molecules. Each solvent molecule occupies one lattice site. Only the exchange movement of monomers is used in the simulations.[31] In an exchange move, a monomer is selected and can exchange with a solvent molecule on one of its 18 nearest neighbors. If the exchange does not break the terpolymer molecule, it is allowed. If the exchange creates a single break in the molecule, the vacancy will continue to exchange with subsequent monomers along the broken chain until reconnection of the links occurs. If the exchange breaks the molecule into more than two parts, it is not allowed. The acceptance or rejection of an attempted move is further governed by the Metropolis rule.[33]

The energy of the system is the objective function of the simulated annealing procedure. In the present paper only the 18 nearest neighbor interactions are considered. These interactions are modeled by assigning an energy $E_{ij} = \varepsilon_{ij} k_B T_{ref}$ to each nearest neighbor pair of components i and j, where $i, j = A, B, C, D$, and S (solvent). Here ε_{ij} is the reduced interaction energy, k_B the Boltzmann constant, and T_{ref} a reference temperature. It is assumed that $\varepsilon_{ii} = 0$ and $\varepsilon_{iD} = 0$, with $i = A, B, C, D$, and S.

The simulations were carried out using a linear annealing schedule, $T_i = fT_{i-1}$, where T_i is the temperature used in the i-th annealing step and f is a scaling factor. The annealing was continued until the number of the annealing steps reachs a predetermined value. Specifically, the initial temperature was set at $T_1 = 120\ T_{ref}$ and 130 annealing steps were used. The scaling factor f was taken as 0.95 or 0.99, depending on the difference of the average energies of the system at the previous two annealing steps. $f = 0.95$ was used when the difference of the average energy is small, and $f = 0.99$ was used when the average energy difference is large. One Monte Carlo step (MCS) is defined as the time taken for, on average, all the lattice sites to be visited for an attempted move. At each annealing step, 9000 MCSs are performed.

For all the simulations reported in this paper, the number of terpolymer molecules and the number of monomers in each molecule are fixed at $N_{Ch} = 360$ and $N = 25$, respectively. The star terpolymers employed in the simulations consist of one solvophilic (A) arm and two solvophobic (B and C) arms. The amphiphilic nature of the polymers are enforced by keeping $\varepsilon_{AS} = -1$, $\varepsilon_{AB} = \varepsilon_{AC} = 1$, $\varepsilon_{BS} > 0$, and $\varepsilon_{CS} > 0$. Furthermore, the two solvophobic arms are assumed to have the same degree of solvent phobicity, i.e., $\varepsilon_{BS} = \varepsilon_{CS}$. This set of interaction parameters is kept as constants in the simulations, ensuring that the solvent is good to the A arm and poor to the B and C arms and that the A and B or C arms are immiscible. Exploration of the phase space is achieved by varying the arm lengths N_i, or equivalently the volume fractions $f_i = N_i/(N-1)$ ($i = A$, B, or C), and the interaction parameters ε_{BS} or ε_{BC}.

Results and Discussion

In this section, the simulation results are presented in terms of morphological phase diagrams, along with discussions and comparisons with available experiments. Different cross sections of the phase diagrams, in terms of three volume fractions (f_A, f_B, and f_C) for a given set of interaction parameters (Figures 1a, S1 and S2) or in terms of the interaction parameters (Figures 2, 3 and S3) for a given set of polymer compositions, are shown first. Chain packing in different micelles is then investigated (Figure 4 and 5). Finally, fine structures of vesicles are presented in Figure 6.

Morphological Phase Diagrams As a Function of Terpolymer Compositions. In the current study, we focus on the case in which the two solvophobic arms are highly incompatible with each other and they are highly insoluble in the solvents. The phase diagram with $\varepsilon_{BS} = 3$ and $\varepsilon_{BC} = 2$ (case 1) in the composition space is shown in Figure 1a, whereas similar phase diagrams with $\varepsilon_{BS} = \varepsilon_{BC} = 2$ (case 2) and $\varepsilon_{BS} = 3$ and $\varepsilon_{BC} = 4$ (case 3) are included in the Supporting Information (Figures S1 and S2, respctively). For clarity and for comparisons with previous experiments, representative snapshots of micelles are given in these phase diagrams. Specifically, representative snapshots of the morphological sequence on the isopleth $f_B = f_C$ are plotted in the top-left and left of each diagram, while representative snapshots with $f_B < f_C$ are plotted at the right.

(28) (a) Kirkpatrick, S.; Gelatt, C. D.; Vecchi, M. P., Jr. *Science* **1983**, *220*, 671. (b) Grest, G. S.; Soukoulis, C. M.; Levin, K. *Phys. Rev. Lett.* **1986**, *56*, 1148.
(29) Carmesin, I.; Kremer, K. *Macromolecules* **1988**, *21*, 2819.
(30) Larson, R. G. *J. Chem. Phys.* **1989**, *91*, 2479. **1992**, *96*, 7904.
(31) Sun, P.; Yin, Y.; Li, B.; Chen, T.; Jin, Q.; Ding, D.; Shi, A.-C. *J. Chem. Phys.* **2005**, *122*, 204905.
(32) Yu, B.; Sun, P.; Chen, T.; Jin, Q.; Ding, D.; Li, B.; Shi, A.-C. *Phys. Rev. Lett.* **2006**, *96*, 138306.
(33) Metropolis, N.; Rosenbluth, A. W.; Rosenbluth, M. N.; Teller, A. H.; Teller, E. *J. Chem. Phys.* **1953**, *21*, 1087.

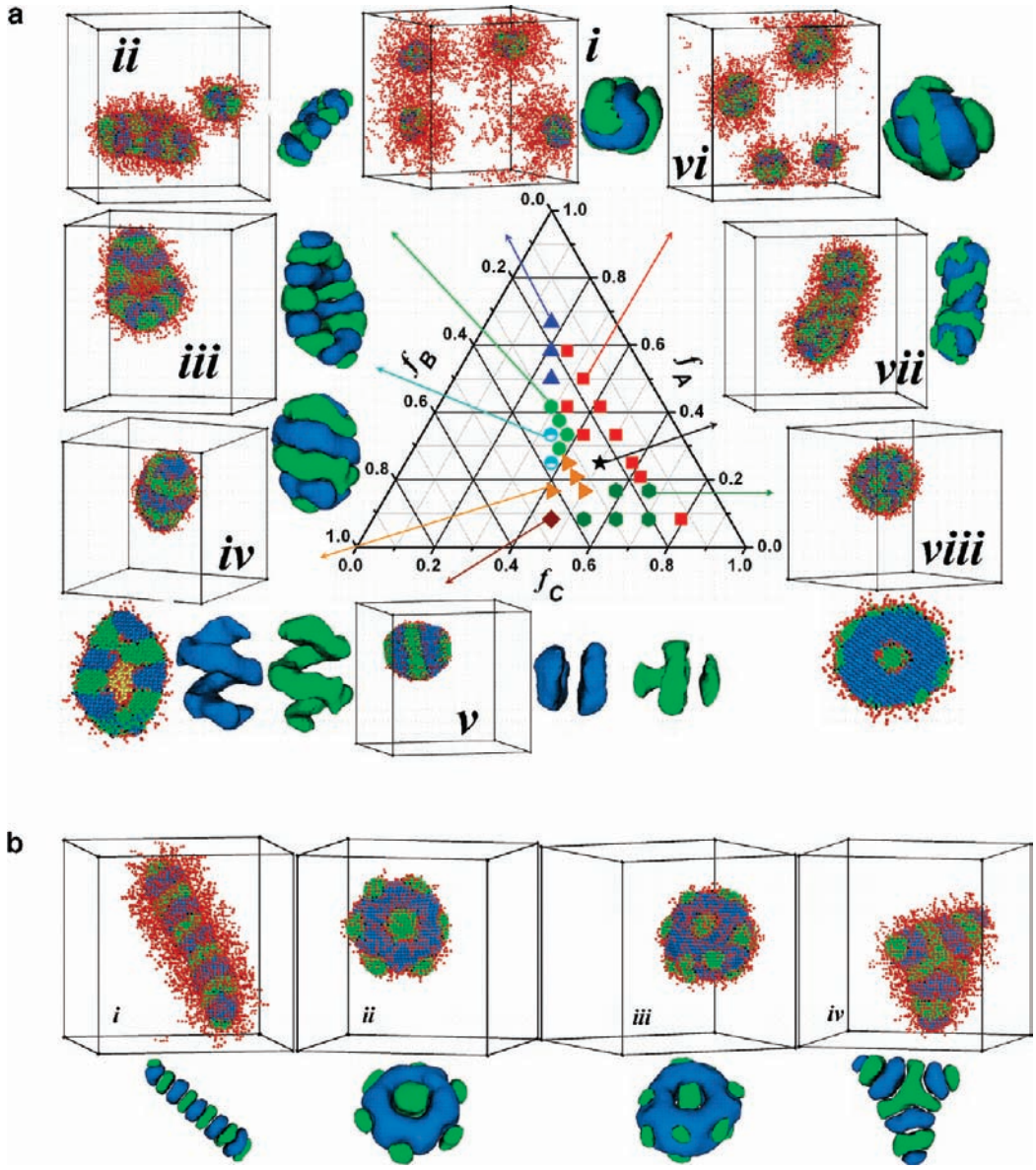

Figure 1. (a) Morphological phase diagram of ABC star terpolymers in selective solvents with $\varepsilon_{BS} = 3$ and $\varepsilon_{BC} = 2$. f_A, f_B, and f_C are the volume fractions of the A, B, and C arms, respectively. The same symbols represent similar morphologies. Representative snapshots of the micellar morphologies are shown. For clarity, a micellar structure, in which the A-arms are removed and/or a cross-sectional view or views with B or C domains only, is shown separately on the right or below the corresponding snapshot. The labels in the snapshots correspond to (*i*) hamburger micelles, (*ii*) segmented bilayer sheets, (*iii*) segmented semivesicles, (*iv*) laterally structured vesicles, (*v*) layer structures, (*vi*) raspberry micelles, (*vii*) multicompartment worms, and (*viii*) multicompartment onions. (b) Typical segmented worms (with $f_A = {}^5/_{12}$, $f_B = {}^1/_4$, and $f_C = {}^1/_3$ (*i*)), disk-like micelles (with $f_A = {}^1/_6$, $f_B = {}^1/_4$, $f_C = {}^7/_{12}$ (*ii*) and $f_A = {}^1/_6$, $f_B = {}^1/_6$, $f_C = {}^2/_3$ (*iii*)), and bilayer sheets (*iv*) (with $f_A = f_B = f_C = {}^1/_3$) obtained when $\varepsilon_{BS} = 3$ and $\varepsilon_{BC} = 4$. The disk-like micelle is in an oblate ellipsoid shape with an internal morphology of nearly hexagonally packed short cylinders or spheres. Color scheme in the snapshots: A (red), B (green), C (blue), junction point (black), and the solvent molecule inside the vesicle (yellow).

Similar to previous experiments and simulations, the phase diagrams obtained from the current simulations reveal a rich variety of morphologies and morphological transitions for the ABC terpolymer solutions. For example, a morphological sequence, hamburger micelles → segmented bilayer sheets → segmented semivesicles → laterally structured vesicles → layer structures, is observed with the decrease of f_A when $f_B \approx f_C$ (Figure 1a). A different morphological sequence, raspberry micelles → multicompartment worms → multicompartment onions, is observed with the decrease of f_A for $f_B < f_C$ (or $f_B > f_C$) (Figure 1a).

Comparing Figure S1 or Figure S2 with Figure 1a, we notice several important differences, despite that the overall tendency of morphological transitions is similar in these three cases. For example, in cases 2 and 3, segmented worms are observed between the hamburger micelles and bilayer sheets along the isopleth $f_B = f_C$, and circular disk-like micelles are observed at $f_A = {}^1/_{12}$ and/or ${}^1/_6$, respectively, for $f_B \ll f_C$. Typical segmented worms, disk-like micelles, and bilayer sheets are shown in Figure 1b. At the same time, laterally segregated semivesicles were not observed in cases 2 and 3. Besides these obvious differences in morphological sequences, the size of the regions occupied by the different micelles and the details in micelle structures are also different among these three cases. These results demonstrate that the final morphology of a given ABC terpolymer depends sensitively on the polymer compositions and polymer−polymer, polymer−solvent interactions.

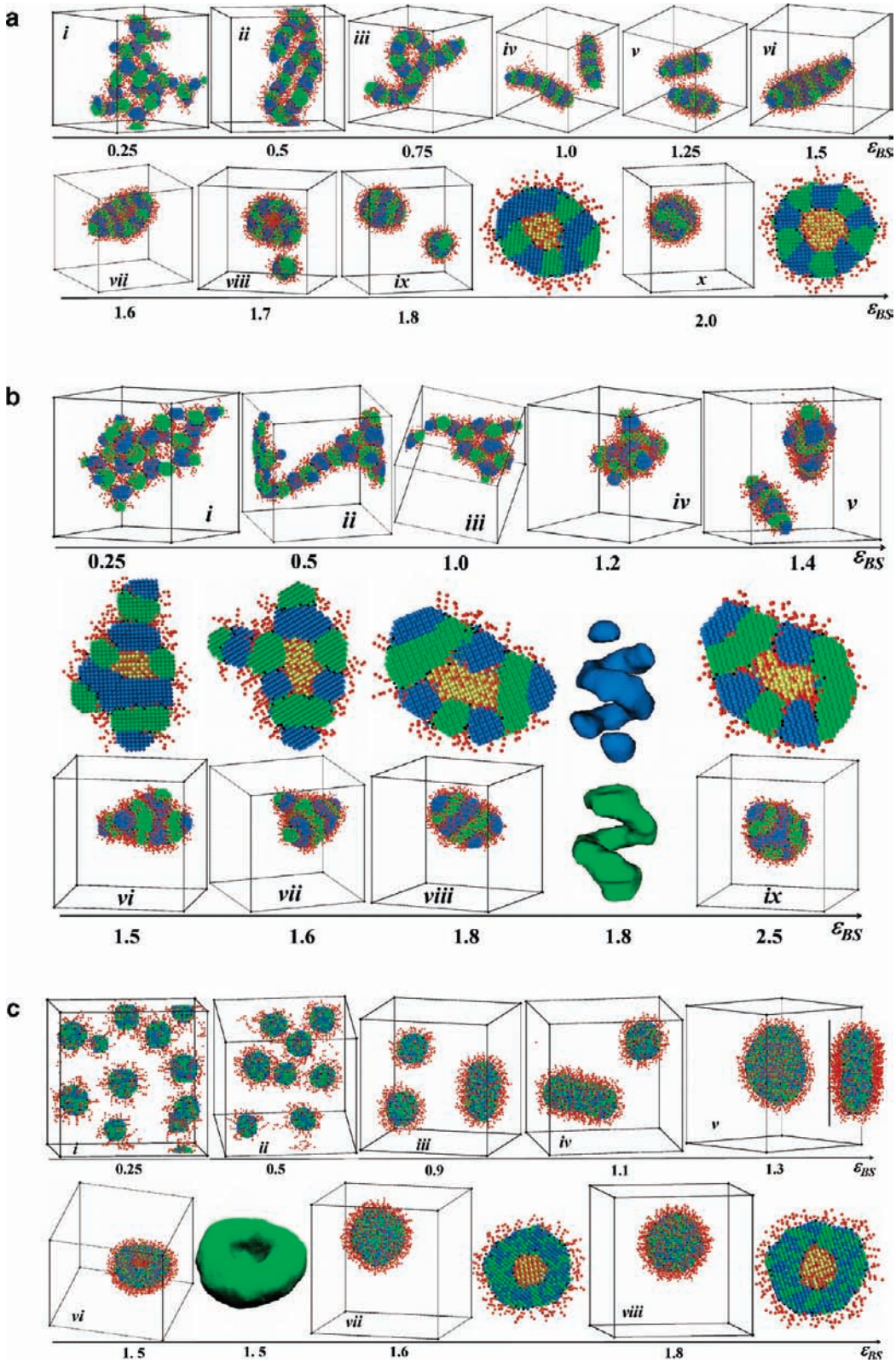

Figure 2. Typical morphologies of a star terpolymer in selective solvents as a function of ε_{BS}, when $f_A = {}^1/_6$, $f_B = f_C = {}^5/_{12}$ and (a) $\varepsilon_{BC} = 1$, (b) $\varepsilon_{BC} = 2$, and (c) $\varepsilon_{BC} = 0$. The color code is the same as that in Figure 1. In (a), the labels correspond to (*i*−*ii*) spheres-on-string networks, (*iii*−*iv*) segmented worms, (*v*−*vi*) laterally segregated flat bilayer sheets, (*vii*−*viii*) structured semivesicles, and (*ix*−*x*) structured vesicles. In (b), (*i*−*iii*) spheres-on-string networks, (*iv*) closely packed spheres-on-string networks, (*v*) bilayer sheets, and (*vi*−*ix*) structured vesicles. In (c), (*i*−*iii*) spherical micelles, (*iv*) mixture of spherical micelles and segmented worms, (*v*) flat bilayer sheets (viewed from two perpendicular directions), (*vi*) semivesicles, and (*vii*−*viii*) vesicles; the green and blue colors are the same.

Despite the complexity of the morphologies and morphological transition sequences, some generic features of the phase behavior of the ABC star terpolymer solutions can be extracted from the phase diagrams. The first generic feature is that the

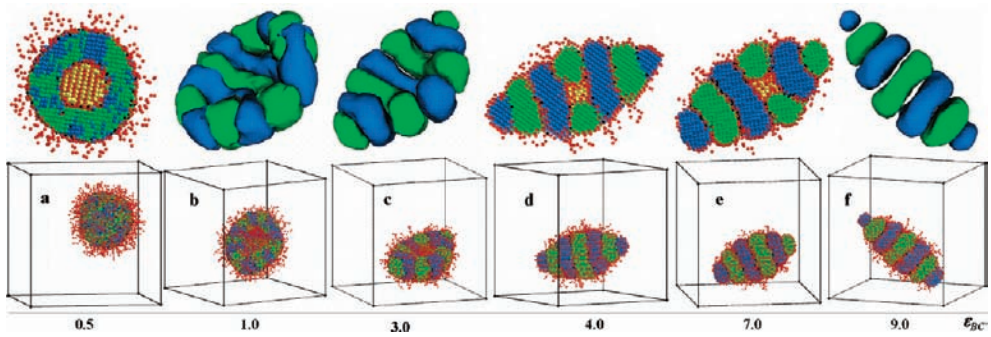

Figure 3. Typical morphologies of the star terpolymers in a selective solvent as a function of ε_{BC}, when $f_A = {}^1/_4$, $f_B = f_C = {}^3/_8$, and $\varepsilon_{BS} = 3$ using the same coloring scheme as that in Figure 1. (a) Vesicles, (b−c) semivesicles, (d−e) vesicles, and (f) layer structures.

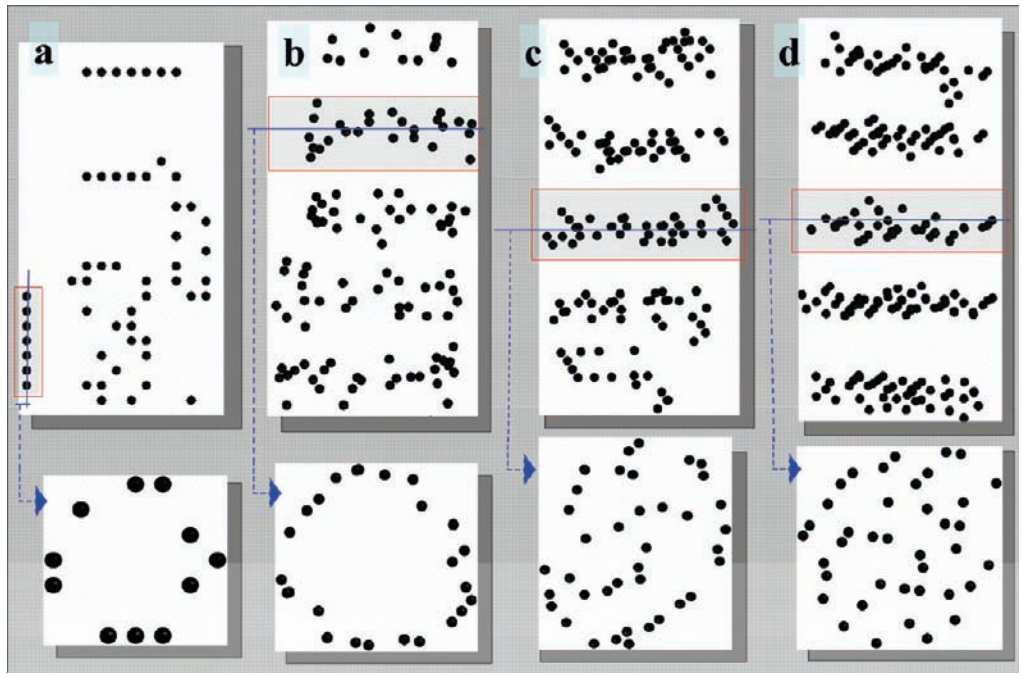

Figure 4. Distribution of junction points in some micelles. For clarity only a part of each micelle is shown. The corresponding micelles are these shown in (a) Figure 2a (i), (b) Figure 2a (iv), (c) Figure S1c, and (d) Figure 1b (i). In the top row, side views are given, while, in the bottom row, cross-sectional views for the boxed parts are shown.

overall tendency of the structural transition is largely governed by the volume fraction of the solvophilic arms. This feature is consistent with the observation that, in terms of the amphiphilic properties, the ABC terpolymers are analogous with A-b-(BC) diblock copolymers. Therefore one expects a transition sequence from spheres to rods to bilayers as the volume fraction of the solvophilic block is decreased.[34] Indeed this morphological sequence is consistent with that observed in Figures 1a, S1 and S2, in which hamburger micelles (spheres), segmented worms (cylinders), structured bilayer sheets, semivesicles, and vesicles are usually obtained with decreasing f_A. This similarity indicates that the general principles governing the phase behavior of diblock copolymer solutions[35,36] could be applied to ABC star terpolymers, with the understanding that the microphase separation between the two solvophobic arms can greatly enrich the micellar morphologies of ABC star terpolymers. The second generic feature of the phase behavior is that the internal morphology in the solvophobic segment domains is largely controlled by the ratio f_B/f_C. This behavior is similar to what happens in BC diblock copolymer melts. For ABC star terpolymers with two equal or nearly equal lengths of solvophobic arms, the morphologies of the solvophobic domains in a variety of micellar structures (the hamburger micelles, segmented worms and sheets, and layer structures) are very similar to the lamellar structures formed by symmetric or nearly symmetric diblock copolymer melts. For ABC star terpolymers with two very different lengths of solvophobic arms, the morphologies of the solvophobic domains in the raspberry micelles and the multicompartment worms or onions or the disk-like micelles are analogues of the spherical or cylindrical phases formed by asymmetric diblock copolymer melts. From these observations, the morphology of the BC arms can be considered as from the self-assembly of BC diblock copolymers confined in the solvophobic domains. The competition between the self-assembly of BC arms and confinement effects lead to a variety of ABC star terpolymer micelles.

(34) Won, Y.-Y.; Brannan, A. K.; Davis, H. T.; Bates, F. S. *J. Phys. Chem. B* **2002**, *106*, 3354.
(35) Halperin, A.; Tirrell, M.; Lodge, T. P. *Adv. Polym. Sci.* **1992**, *100*, 31.
(36) Zhulina, E. B.; Adam, M.; LaRue, I.; Sheiko, S. S.; Rubinstein, M. *Macromolecules* **2005**, *38*, 5330.

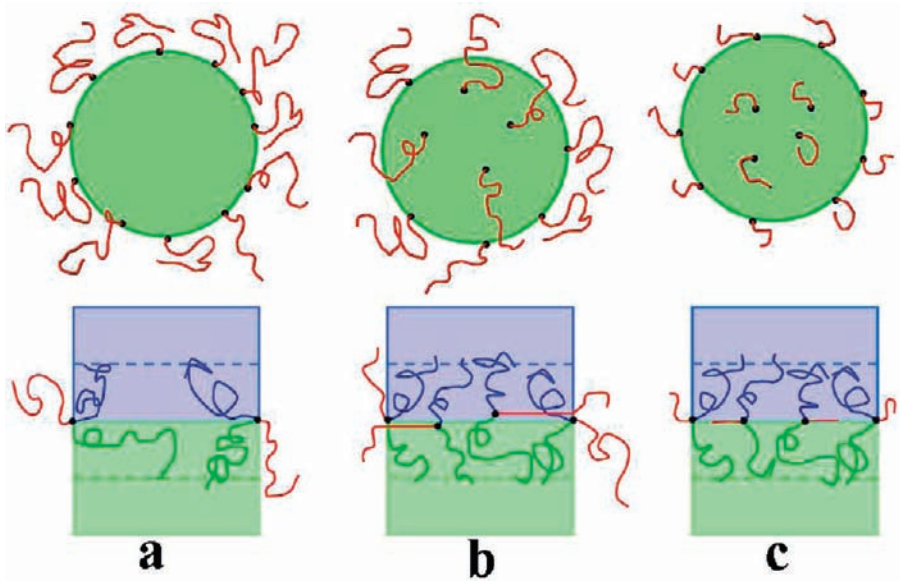

Figure 5. Schematic chain packings in different micelles: (a) when ε_{BC} is smaller than or about equal to ε_{AB} and ε_{AC}. (b) and (c) when ε_{BC} is much larger than ε_{AB} and ε_{AC}. For clarity, the internal junction points in (b) are plotted to be slightly deviated from the interfacial plane. The color code is the same as that in Figure 1.

It is interesting to note that, although the topology of the overall shape of the micelles is largely determined by the volume fraction of the solvophilic A arm, the details of the overall shape of the micelles depend on the internal structures. For example, the bilayer sheets are elliptical, elongated along the direction perpendicular to the small lamellae in cases 1 and 2 (Figures 1a and S1). Furthermore, triangular bilayer sheets are found in case 3 (Figures 1b and S2). On the other hand, circular bilayer sheets can be obtained, such as the disk-like micelles observed in Figures 1b, S1, and S2 in the case when $f_B \ll f_C$. From these observations it can be concluded that the overall shape of the micelles is determined by the interplay between the volume fraction of the A arm and the internal structure.

We have carried out extensive simulations for the model system under a variety of conditions. The results demonstrate that the three phase diagrams given in Figures 1a, S1, and S2 are generic, representing three typical cases with $\varepsilon_{BS} > \varepsilon_{BC}$, $\varepsilon_{BS} \approx \varepsilon_{BC}$, and ε_{BS} is slightly smaller than ε_{BC}. Any ABC star terpolymer belonging to one of these three cases exhibits phase behavior similar to the corresponding phase diagram shown in these figures, whereas with simple displacement of the phase regions. Specifically, the phase regions in the corresponding phase diagram shown in Figures 1a, S1, or S2 are shifted to larger f_A values, and the region of vesicles will become large for a large value of ε_{BS}, whereas the phase regions are moved to smaller f_A values and the region of vesicles will become small or even disappear for a small value of ε_{BS}. On the other hand, the region of layer structures will become large for a large value of ε_{BC}.

The simulation results are in excellent agreement with experiments by Lodge et al. on μ-EOF miktoarm star terpolymers in aqueous solutions.[16−18] The simulations reproduced all the experimentally observed novel morphologies, including the hamburger micelles, segmented worms, nanostructured bilayer sheets, nearly completely closed vesicles and a large proportion of fully formed vesicles, raspberry-like micelles, and multicompartmentalized worms. Furthermore, the predicted morphological phase diagrams are consistent with the experimental one. The small protrusions on the side surface of bilayer sheets or on the outside surface of vesicles (Figure S1e−f) are similar to the protruding tails observed experimentally by Lodge et al.[17] On the other hand, our simulations predicted some novel lateral structures and some new micelles, such as helices or stacked donuts for vesicles, segmented semivesicles and bilayer sheets, and multicompartment disks and onions, which have yet to be observed in experiments.

Morphological Phase Diagrams As a Function of the Interaction Parameters. The effects of polymer−polymer and polymer−solvent interactions on the phase behavior are examined in this subsection. For the star terpolymer with $f_A = {}^1/_6$ and $f_B = f_C = {}^5/_{12}$, three series of typical micelle morphologies as a function of ε_{BS} are shown in Figure 2 with different values of ε_{BC}. Figure 2a shows that, for the case of $\varepsilon_{BC} = 1$, structured vesicles start to form when ε_{BS} is large enough ($\varepsilon_{BS} \geq 1.8$), whereas segmented worms are observed for small values of ε_{BS} ($0.5 < \varepsilon_{BS} \leq 1.0$). For even smaller values of ε_{BS} ($0 < \varepsilon_{BS} \leq 0.5$), spheres-on-string networks are obtained. For intermediate values of ε_{BS} ($1.2 < \varepsilon_{BS} \leq 1.7$), laterally segregated flat bilayer sheets and semivesicles, shaped as ellipses and as boats or bowls, respectively, are observed. The spheres-on-string networks are similar to the segmented worms in appearance, but they differ in details. In the spheres-on-string networks, the B and C arms form spheres which are linked in an alternating arrangement due to the linkage of the B and C arms at the junction point. On the other hand, in a segmented worm, the B (C) arms form disk-like layers. Using Monte Carlo simulations, Zhu et al. observed what is termed pearl-necklace micelles at relatively low polymer concentration,[22] which is a structure similar to the spheres-on-string networks. Combining the observations from Figures 1a and 2a, we conclude that similar morphological sequences, from segmented worms to segmented bilayer sheets and then to laterally structured semivesicles and vesicles, can be induced by either decreasing f_A or increasing ε_{BS}. Because the effect of decreasing f_A or increasing ε_{BS} is to enhance the solvophobic interaction, it is expected that the two morphological sequences shown Figures 1a and 2a are similar.

Figure 2b shows that when $\varepsilon_{BC} = 2$, spheres-on-string networks appear for small values of ε_{BS} ($\varepsilon_{BS} < 1.2$), whereas structured vesicles are formed for large values of ε_{BS} ($\varepsilon_{BS} \geq$

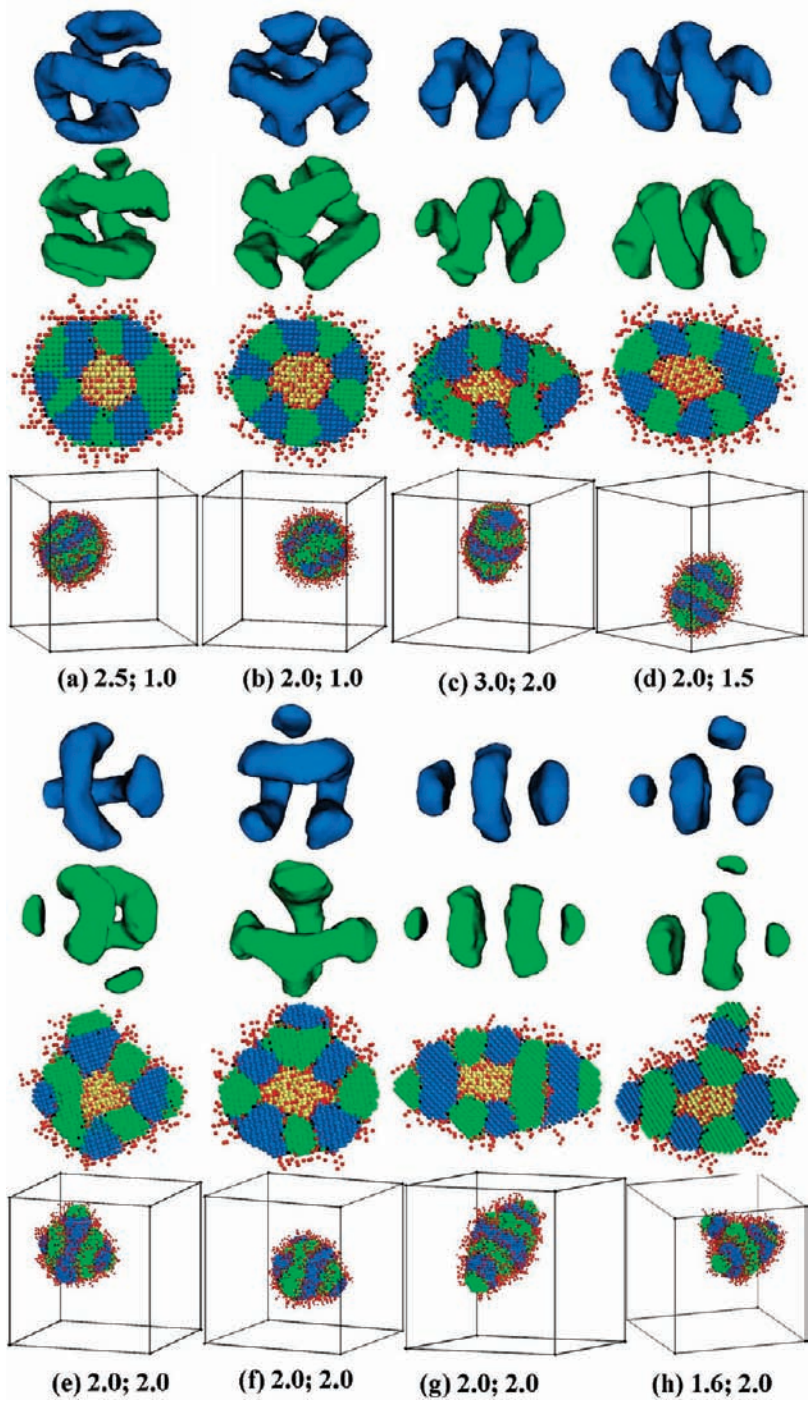

Figure 6. Vesicle morphologies obtained for system with $f_A = {}^1/_6$ and $f_B = f_C = {}^5/_{12}$ as a function of ε_{BS} and ε_{BC}. The corresponding ε_{BS} and ε_{BC} values are labeled below each snapshot. The color code is the same as that in Figure 1.

1.5). For intermediate ε_{BS} values ($1.2 \leq \varepsilon_{BS} \leq 1.3$), the observed morphologies are closely packed spheres-on-string networks, where some B or C spheres at the center of the networks are merged together. When $\varepsilon_{BS} = 1.4$, a flat bilayer sheet with two small protrusions, one on each side of the sheet, is formed. In Figure 2b, it is interesting to notice that vesicles are formed with the increase of ε_{BS} without a semivesicle region, in contrast to the case shown in Figure 2a.

Comparing Figure 2c with Figure 2a reveals that the morphological sequence with $\varepsilon_{BC} = 0$ is similar to that with $\varepsilon_{BC} = 1$, with a number of differences. One prominent difference is that the B and C arms are mixed in the morphologies shown in Figure 2c, whereas they are separated in Figure 2a. Another difference is that the shape of the bilayer sheet is disk-like in Figure 2c(v), whereas it is elliptic in Figure 2a($v-vi$). A disk-like shape can decrease the contact between the solvophobic arms and the solvent, since the circular sheet can minimize the exposed edge.[37] On the other hand, a noncircular sheet can decrease the contact between the two solvophobic arms. Therefore, it is the nonzero ε_{BC} value that drives the formation of the noncircular bilayer sheets.

(37) Weiss, T. M.; Narayanan, T.; Wolf, C.; Gradzielski, M.; Panine, P.; Finet, S.; Helsby, W. I. *Phys. Rev. Lett.* **2005**, *94*, 038303.

The results presented in Figure 2 demonstrate clearly that the degree of solvent phobicity (ε_{BS}) has a large influence on the micellar morphology. When ε_{BS} is large enough, vesicles are formed in all cases. It is interesting to note that, when all the interaction parameters are kept as constants, the minimal ε_{BS} value to form vesicles, defined as ε_V, is very sensitive to the star terpolymer compositions. From simulation results with different polymer compositions, it is observed that ε_V is an increasing function of f_A. Furthermore, for a terpolymer with $f_B = f_C$, a morphological sequence similar to that shown in Figure 2a can be obtained with the increase of ε_{BS} when $\varepsilon_V > \varepsilon_{BC}$. In this case, a larger ($\varepsilon_V - \varepsilon_{BC}$) value is associated with a larger region of the laterally segregated semivesicles. On the other hand, a morphological sequence similar to that shown in Figure 2b can be obtained with the increase of ε_{BS} when $\varepsilon_V < \varepsilon_{BC}$.

The formation of different structures by the ABC star terpolymers is driven by the competition between the different interactions. In the limiting case of $\varepsilon_{BC} = 0$, the system always satisfies $\varepsilon_V > \varepsilon_{BC}$, which is the reason that the sequence shown in Figure 2c is similar to that shown in Figure 2a. In the case of Figure 2c, the B and C arms are chemically identical, corresponding to surfactants with two hydrophobic tails. When the solvent quality for the hydrophobic segments is decreased, a morphological sequence, from spheres to cylinders and then to vesicles, has been observed in surfactant and diblock copolymer systems.[38,39] This is consistent with the morphological sequence shown in Figure 2c, except that bilayer sheets and semivesicles are also observed in a narrow region in Figure 2c. For a nonzero ε_{BC}, the B and C arms are separated in the BC domains. When ε_{BC} is relatively small ($\varepsilon_V/\varepsilon_{BC} > 1$), a morphological sequence identical to that for $\varepsilon_{BC} = 0$ is predicted (Figure 2a). However, the spheres, cylinders, and vesicles are transformed to the spheres-on-string networks, segmented worms, and structured vesicles, respectively, due to the separation between the two solvophobic arms when $\varepsilon_{BC} > 0$. Another difference is that the ε_V value becomes slightly larger in the system with $\varepsilon_{BC} = 1$ than that with $\varepsilon_{BC} = 0$ (see Figure 2a and 2c). This indicates that the microphase separation between the two solvophobic arms can delay the formation of vesicles to a large ε_V value. On the other hand, the value of ε_V becomes slightly smaller in the system with $\varepsilon_{BC} = 2$ than that with $\varepsilon_{BC} = 0$ (see Figure 2b and 2c), due to the fact that when ε_{BC} is large enough, a fraction of the solvophilic arms can penetrate between the two solvophobic arms to shield their contact, as demonstrated from the cross-sectional views of the vesicle structures shown in Figure 2b. The shielding effect leads to a smaller effective volume fraction of the solvophilic arm. As mentioned earlier, ε_V is an increasing function of f_A; thus a decrease in the effective f_A leads to a decrease in ε_V value. On the other hand, in the system with a large ε_{BC}, the ε_{BS} region for spheres-on-string networks is enlarged due to the strong incompatibility between the two solvophobic arms. Combining these two effects, the spheres-on-string networks can transform to vesicle structures with increasing ε_{BS} without a region of semivesicles in systems with large ε_{BC} values (see Figure 2b).

Figure 2 shows that the morphology of multicompartment micelles also relies on the repulsive interaction between the two solvophobic arms (ε_{BC}). Typical morphologies as a function of ε_{BC} for two star terpolymers with different f_A are presented in Figures 3 and S3. Figure 3 shows that vesicles are formed when $\varepsilon_{BC} \leq 0.5$, whereas layer structures are formed when $\varepsilon_{BC} > 7.0$. The aspect ratio of the layer structure is increasing with the increase of ε_{BC}. For intermediate ε_{BC} values ($1 \leq \varepsilon_{BC} \leq 3$), laterally segregated semivesicles are observed. Furthermore, ellipsoid shaped vesicles are observed when $4.0 \leq \varepsilon_{BC} \leq 7.0$. In the sequence shown in Figure S3, vesicles are formed when $\varepsilon_{BC} \leq 2.0$, and layer structures are formed when $\varepsilon_{BC} > 2.0$. This sequence is similar to that shown in Figure 3, but without a semivesicle region. Our extensive simulations demonstrate that, for an arbitrary star terpolymer with $f_B = f_C$, a morphological sequence similar to that shown in Figure 3 or S3 is obtained with the increase of ε_{BC}. The semivesicles may or may not occur depending on the volume fraction of the solvophilic arms.

The predicted morphological sequences as a function of ε_{BC} reveal the effect of the competition between the different interactions. In the limiting case of large ε_{BC}, a large portion of the solvophilic A arms is penetrating between the two solvophobic arms to shield their contact (see Figure 3), resulting in a relatively smaller effective volume fraction of the A arm. Similar to the case shown in Figure 1a, a decrease in the effective f_A leads to the formation of layer structures and/or larger region of the layer structures (Figure S2). On the other hand, in the limiting case of $\varepsilon_{BC} = 0$, vesicles are formed when ε_{BS} is large enough (as shown in Figure 2c). A morphological sequence from vesicles and finally to layer structures can be obtained with increasing ε_{BC}. For moderate values of ε_{BC}, separation of the B and C domains occurs. Similar to the behavior shown in Figure 2a, a relatively small value of ε_{BC} can delay the occurrence of vesicles to a larger ε_V, and therefore for a terpolymer that forms vesicles when $\varepsilon_{BC} = 0$, semivesicles may occur instead of vesicles for moderate values of ε_{BC}. A further increase of ε_{BC} leads to a portion of the solvophilic A-arms penetrating between the two solvophobic arms. When ε_{BC} is large enough, the number of the penetrating A arms increases with the further increase of ε_{BC}. Therefore, the effective volume fraction of the A arms decreases suddenly at a certain ε_{BC} value, and when ε_{BC} is larger than that value, it decreases with the further increase of ε_{BC}, leading to the occurrence of vesicles and layer structures. Such a morphological sequence with increasing ε_{BC} corresponds to that observed in Figure 3, which is consistent with the sequence of decreasing f_A when $f_B \approx f_C$ shown in Figure 1a. On the other hand, for systems with small f_A, vesicles are stable for a relatively large ε_{BC} region, which may lead to missing the semivesicle region, similar to that shown in Figure S3.

Chain Packing. To gain insight into the packing of polymer chains into the various structures, we investigated the distributions of junction points in different micellar morphologies. Some representative results are shown in Figure 4. Due to the particular chain architectures of *ABC* miktoarm star terpolymers, their junction points must be located on the mutual intersections of the A, B, and C domains. On the other hand, our results show that the distribution of junction points depends on the interaction parameters. In the case when ε_{BC} is smaller than or about equal to ε_{AB} and ε_{AC}, the mutual intersections are equivalent to the intersections between the BC interfaces and the micelle−solvent interface. In this small ε_{BC} case, the intersections are circles. Our results show that when ε_{BS} is much smaller than ε_{BC}, e.g., $\varepsilon_{BS} = 0.25$, the junctions do form circles and each circle is on a plane (Figure 4a), whereas when ε_{BS} is comparable to or larger than ε_{BC}, e.g., $\varepsilon_{BS} = 1.0$, the junctions also form circles but the side view of each circle is a band (Figure 4b). In the case when ε_{BC} is much larger than ε_{AB} and ε_{AC}, e.g., $\varepsilon_{BC} = 4$, the junction points are also located on the internal BC interfaces in addition to the micelle−solvent interface (Figure 4d), due to the fact that a fraction of the solvophilic arms can penetrate between

(38) Shen, H.; Eisenberg, A. *J. Phys. Chem. B* **1999**, *103*, 9473.
(39) Burke, S. E.; Eisenberg, A. *Langmuir* **2001**, *17*, 6705.

the two solvophobic arms. Between the two limiting cases, the number of the junctions located on the internal BC interfaces decreases with the decrease of ε_{BC} (Figure 4c).

Schematics of chain packing in some representative micelles are shown in Figure 5. The chain packing is closely related to the distributions of junctions. Figure 5a represents the case when ε_{BC} is smaller than or about equal to ε_{AB} and ε_{AC}. In this case, all the solvophilic A-arms emanate from the BC interfaces, they anchored around circles (Figure 4a) or band circles (Figure 4b) formed by the junctions and are in contact with solvents. Within the solvophobic B or C domains, some of the B or C arms tend to orientated nearly perpendicular to the interfaces, while others orientated randomly. We computed the angle φ to provide detailed information about chain packing, where φ is defined as the angle between the vectors from the junction point to the centers of mass of B and C arms. We find that in this small ε_{BC} case, there are more than 90% chains with a φ value between 90−180 °C when $\varepsilon_{BS} = 0.25$, this ratio decreases with the increase of ε_{BS}, and it is about 30% when $\varepsilon_{BS} = 1.0$. In the latter case, there are more than 80% chains with a φ value between 45−110 °C.

Figure 5b and 5c represent the case when ε_{BC} is much larger than ε_{AB} and ε_{AC}. In this case, the junctions are also located on the internal BC interfaces, besides on the intersections between the BC interfaces and the micelle−solvent interface. When f_A is not very small, the size of each BC interface is usually not too large so that most of each of these A arms with internal junctions can emanate from the BC interfaces and are in contact with solvents (Figure 5b). When f_A is very small, the size of each BC interface is usually large and these A arms with internal junctions usually cannot emanate (Figure 5c). Therefore, there are A segments on the internal BC interfaces in this large ε_{BC} case. However, the thickness of the A segment between B and C domains is always very thin because when f_A is small, the fraction of internal A segments is small, while when f_A is large, only a small fraction of each of these internal A arms remains. We also find that in this limiting case of large ε_{BC}, there are more than 85% chains with a φ value between 90 and 180 °C when $f_A = {}^1/_6$, $\varepsilon_{BS} = 3$, and $\varepsilon_{BC} = 4$. This ratio decreases with either the increase of f_A or the decrease of ε_{BS}; it is ∼60% when $f_A = {}^7/_{12}$, $\varepsilon_{BS} = 3$, and $\varepsilon_{BC} = 4$ and ∼46% when $f_A = {}^1/_6$, $\varepsilon_{BS} = 3$, and $\varepsilon_{BC} = 2$. Our further investigations show that chain packing in the other micelles is similar to those illustrated in Figure 5, except that the section shape is different.

Vesicle Structures. Results from Figures 1−3 and S1−S3 indicate that the lateral structures and shapes of vesicles are complex. When ε_{BC} is much small, the B and C arms are not well segregated in the vesicle shell (see snapshots with $\varepsilon_{BC} = 0.5$ in Figures 3 and S3). In this case, the outside surface of a vesicle is smooth and the overall shape is spherical. When ε_{BC} is comparable with ε_{BS}, vesicles with well segregated B and C domains are observed, and typical snapshots are shown in Figure 6. In the case when ε_{BC} is slightly smaller than ε_{BS}, vesicles usually consist of B and C helices, including both single and double helices (Figure 6a−d). In this case, the outside surface of a vesicle is still smooth but the overall shape is usually not spherical but slightly elongated along the helical axis. The formation of helices is due to the existence of competing interactions in these ABC miktoarm star terpolymer−solvent systems. In the case when ε_{BC} is slightly larger than ε_{BS}, vesicles are in prolate ellipsoids shapes, consisting of stacked B and C donuts in the central part and B and C disks on the boundary (Figure 6h). In the intermediate case when $\varepsilon_{BC} = \varepsilon_{BS}$, vesicles are usually multiple degenerated (Figure 6e−g). These degenerated morphologies can be classified into two types. The first type corresponds to the case in which the vesicles are nearly spherical in shape, where one solvophobic arm forms a hand-shake or connected structure and the other forms a saddle-like structure (Figure 6e−f). The second type corresponds to the case in which the vesicles are in prolate ellipsoid shapes (Figure 6g), similar to those obtained when ε_{BC} is slightly larger than ε_{BS} (Figure 6h). We also noticed that for vesicles obtained when $\varepsilon_{BC} \approx \varepsilon_{BS}$, their outside surfaces are usually with small protrusions instead of smooth. This is also the result of competion between the different interactions. The richness of vesicle shapes is another example illustrating the conclusion that the details of the overall shape of micelles depend on the internal structures.

Conclusion

We have systemically investigated the self-assembly of amphiphilic ABC star terpolymers in an A arm selective solvent using a simulated annealing technique. It is shown that the star terpolymers can spontaneously self-assemble to form various micellar structures. Through controlling the volume fraction of the A arm, the solvent quality, or the incompatibility between the two solvophobic arms, generic phase diagrams and multiple morphological transitions are obtained. Novel micellar structures such as vesicles with lateral structures of helices or stacked donuts, segmented semivesicles, noncircular bilayer sheet, and disk-like micelles are predicted. Chain packing in different micelles is investigated.

Despite the complexity of the phases and phase transitions observed in the system, two generic features of the phase behavior are obtained. The overall geometry of the micellar aggregates is largely controlled by the length of the solvophilic blocks (A-arms). When f_A is decreased, the overall morphology changes from sphere-like (zero-dimensional) to cylinder-like (one-dimensional) to layer-like (two-dimensional) structures. This morphological sequence is similar to that observed in amphiphilic diblock copolymer solutions. On the other hand, the multicompartment morphology of the solvophobic BC domains is mainly controlled by the B/C lengths, as well as BC interactions. The morphological transition within the BC domains can be regarded as from the confined self-assembly of B−C diblock copolymers. The systematic phase diagrams obtained in the current study are consistent with all available experimental and theoretical observations. Furthermore, a number of new morphologies has been predicted.

Acknowledgment. This work was supported by the National Natural Science Foundation of China (Grants No. 20774052 and 20474034), the Chinese Ministry of Education with the Program of New Century Excellent Talents in Universities (Grant No. ncet-05-0221), the Program of Joint-Research Foundation of Nankai and Tianjin Universities, and Nankai University ISC. A.-C.S. gratefully acknowledges the support from the Natural Sciences and Engineering Research Council (NSERC) of Canada.

Supporting Information Available: Morphological phase diagrams with $\varepsilon_{BS} = \varepsilon_{BC} = 2$, and with $\varepsilon_{BS} = 3$, $\varepsilon_{BC} = 4$, and typical morphologies as a function of ε_{BC} when $f_A = {}^1/_6$, $f_B = f_C = {}^5/_{12}$, and $\varepsilon_{BS} = 2$, for ABC star terpolymers in a selective solvent. This material is available free of charge via the Internet at http://pubs.acs.org.

JA900405R